

PARTICLE DETECTORS

To reduce the size of this section's PostScript file, we have divided it into three PostScript files. We present the following index:

PART 1

Page #	Section name
1	25.1 Organic scintillators—by K. Johnson (FSU)
5	25.2 Inorganic scintillators—by C.L. Woody (BNL)
5	25.3 Čerenkov detectors—by D.G. Coyne (UCSC)
8	25.4 Transition radiation detectors (TRD's)—by D. Froidevaux (CERN)
10	25.5 Silicon photodiodes and particle detectors—by H.F.W. Sadrozinski (UCSC) and H.G. Spieler (LBNL)
11	25.6 Proportional and drift chambers

PART 2

Page #	Section name
13	25.7 Time-projection chambers—by M.T. Ronan (LBNL)

PART 3

Page #	Section name
16	25.8 Calorimeters
18	25.9 Measurement of particle momenta in a uniform magnetic field
20	25.10 Superconducting solenoids for collider detectors by R.D. Kephart (FNAL)
22	25.11 Other observations
22	References

16 25. Particle detectors

25.8. Calorimeters

Electromagnetic calorimeters: The development of electromagnetic showers is discussed in the “Passage of Particles Through Matter” section (Sec. 23 of this *Review*). Formulae are given for the approximate description of average showers, but since the physics of electromagnetic showers is well understood, detailed and reliable Monte Carlo simulation is possible. EGS4 has emerged as the standard [50].

The resolution of sampling calorimeters (hadronic and electromagnetic) is usually dominated by sampling fluctuations, leading to fractional resolution σ/E scaling inversely as the square root of the incident energy. Homogenous calorimeters, such as solid NaI(Tl), will in general not have resolution varying as $1/\sqrt{E}$. At high energies deviations from $1/\sqrt{E}$ occur because of noise, pedestal fluctuations, nonuniformities, calibration errors, and incomplete shower containment. Such effects are usually included by adding a constant term to σ/E , either in quadrature or (incorrectly) directly. In the case of the hadronic cascades discussed below, noncompensation also contributes to the constant term.

In Table 25.4 we give resolution as measured in detectors using typical EM calorimeter technologies. In almost all cases the installed calorimeters yield worse resolution than test beam prototypes for a variety of practical reasons. Where possible actual detector performance is given. For a fixed number of radiation lengths, the FWHM in sandwich detectors would be expected to be proportional to \sqrt{t} for t (= plate thickness) ≥ 0.2 radiation lengths [51].

Given sufficient transverse granularity early in the calorimeter, position resolution of the order of a millimeter can be obtained.

Table 25.4: Resolution of typical electromagnetic calorimeters. E is in GeV.

Detector	Resolution
NaI(Tl) (Crystal Ball [52]; 20 X_0)	$2.7\%/E^{1/4}$
Lead glass (OPAL [53])	$5\%/\sqrt{E}$
Lead-liquid argon (NA31 [54]; 80 cells: 27 X_0 , 1.5 mm Pb + 0.6 mm Al + 0.8 mm G10 + 4 mm LA)	$7.5\%/\sqrt{E}$
Lead-scintillator sandwich (ARGUS [55], LAPP-LAL [56])	$9\%/\sqrt{E}$
Lead-scintillator spaghetti (CERN test module) [57]	$13\%/\sqrt{E}$
Proportional wire chamber (MAC; 32 cells: 13 X_0 , 2.5 mm typemetal + 1.6 mm Al) [58]	$23\%/\sqrt{E}$

Hadronic calorimeters [59,60]: The length scale appropriate for hadronic cascades is the nuclear interaction length, given very roughly by

$$\lambda_I \approx 35 \text{ g cm}^{-2} A^{1/3} . \quad (25.18)$$

Longitudinal energy deposition profiles are characterized by a sharp peak near the first interaction point (from the fairly local deposition of EM energy resulting from π^0 's produced in the first interaction), followed by a more gradual development with a maximum at

$$x/\lambda_I \equiv t_{\max} \approx 0.2 \ln(E/1 \text{ GeV}) + 0.7 \quad (25.19)$$

as measured from the front of the detector.

The depth required for containment of a fixed fraction of the energy also increases logarithmically with incident particle energy. The thickness of iron required for 95% (99%) containment of cascades induced by single hadrons is shown in Fig. 25.5 [61]. Two of the sets of data are from large neutrino experiments, while the third is from a commonly used parametrization. Depths as measured in nuclear interaction lengths presumably scale to other materials. From the same data it can be concluded that the requirement that 95% of the energy in 95% of the showers be contained requires 40 to 50 cm (2.4 to 3.0 λ_I) more material than for an average 95% containment.

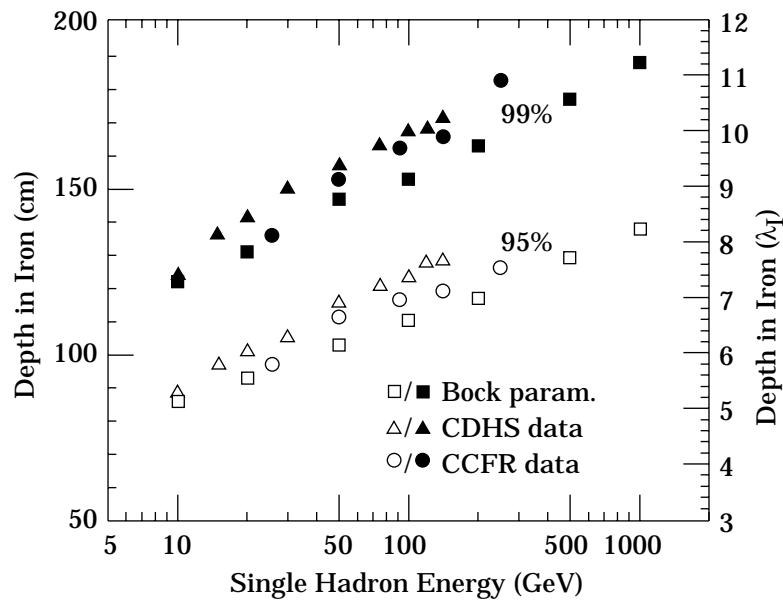


Figure 25.5: Required calorimeter thickness for 95% and 99% hadronic cascade containment in iron, on the basis of data from two large neutrino detectors and the parametrization of Bock *et al.* [61].

The transverse dimensions of hadronic showers also scale as λ_I , although most of the energy is contained in a narrow core.

The energy deposit in a hadronic cascade consists of a prompt EM component due to π^0 production and a slower component mainly due to low-energy hadronic activity. In general, these energy depositions are converted to electrical signals with different

18 25. Particle detectors

efficiencies [62]. The ratio of the conversion efficiencies is usually called the intrinsic e/h ratio. If $e/h = 1.0$ the calorimeter is said to be *compensating*. If it differs from unity by more than 5% or 10%, detector performance is compromised because of fluctuations in the π^0 content of the cascades. Problems include:

- a) A skewed signal distribution;
- b) A response ratio for electrons and hadrons (the “ e/π ratio”) which is different from unity and depends upon energy;
- c) A nonlinear response to hadrons (the response per GeV is proportional to the reciprocal of e/π);
- d) A constant contribution to detector resolution, almost proportional to the degree of noncompensation. The coefficient relating the constant term to $|1 - e/h|$ is 14% according to FLUKA simulations, and 21% according to Wigman’s calculations [59].

In most cases e/h is greater than unity, particularly if little hydrogen is present or if the gate time is short. This is because much of the low-energy hadronic energy is “hidden” in nuclear binding energy release, low-energy spallation products, *etc.* Partial correction for these losses occurs in a sampling calorimeter with thick plates, because a disproportionate fraction of electromagnetic energy is deposited in the inactive region. For this reason, a fully sensitive detector such as BGO or glass cannot be made compensating.

Compensation has been demonstrated in calorimeters with 2.5 mm scintillator sheets sandwiched between 3 mm depleted uranium plates [64] or 10 mm lead plates [65]; resolutions σ/E of $0.34/\sqrt{E}$ and $0.44/\sqrt{E}$ were obtained for these cases (E in GeV). The former was shown to be linear to within 2% over three orders of magnitude in energy, with approximately Gaussian signal distributions.

25.9. Measurement of particle momenta in a uniform magnetic field [71,72]

The trajectory of a particle with momentum p (in GeV/ c) and charge ze in a constant magnetic field \vec{B} is a helix, with radius of curvature R and pitch angle λ . The radius of curvature and momentum component perpendicular to \vec{B} are related by

$$p \cos \lambda = 0.3 z B R , \quad (25.20)$$

where B is in tesla and R is in meters.

The distribution of measurements of the curvature $k \equiv 1/R$ is approximately Gaussian. The curvature error for a large number of uniformly spaced measurements on the trajectory of a charged particle in a uniform magnetic field can be approximated by

$$(\delta k)^2 = (\delta k_{\text{res}})^2 + (\delta k_{\text{ms}})^2 , \quad (25.21)$$

where δk = curvature error

δk_{res} = curvature error due to finite measurement resolution

δk_{ms} = curvature error due to multiple scattering.

If many (≥ 10) uniformly spaced position measurements are made along a trajectory in a uniform medium,

$$\delta k_{\text{res}} = \frac{\epsilon}{L'^2} \sqrt{\frac{720}{N+4}}, \quad (25.22)$$

where N = number of points measured along track

L' = the projected length of the track onto the bending plane

ϵ = measurement error for each point, perpendicular to the trajectory.

If a vertex constraint is applied at the origin of the track, the coefficient under the radical becomes 320.

For arbitrary spacing of coordinates s_i measured along the projected trajectory and with variable measurement errors ϵ_i the curvature error δk_{res} is calculated from:

$$(\delta k_{\text{res}})^2 = \frac{4}{w} \frac{V_{ss}}{V_{ss}V_{s^2s^2} - (V_{ss^2})^2}, \quad (25.23)$$

where V are covariances defined as $V_{s^m s^n} = \langle s^m s^n \rangle - \langle s^m \rangle \langle s^n \rangle$ with $\langle s^m \rangle = w^{-1} \sum (s_i^m / \epsilon_i^2)$ and $w = \sum \epsilon_i^{-2}$.

The contribution due to multiple Coulomb scattering is approximately

$$\delta k_{\text{ms}} \approx \frac{(0.016)(\text{GeV}/c)z}{Lp\beta \cos^2 \lambda} \sqrt{\frac{L}{X_0}}, \quad (25.24)$$

where p = momentum (GeV/ c)

z = charge of incident particle in units of e

L = the total track length

X_0 = radiation length of the scattering medium (in units of length; the X_0 defined elsewhere must be multiplied by density)

β = the kinematic variable v/c .

More accurate approximations for multiple scattering may be found in the section on Passage of Particles Through Matter (Sec. 23 of this *Review*). The contribution to the curvature error is given approximately by $\delta k_{\text{ms}} \approx 8s_{\text{plane}}^{\text{rms}}/L^2$, where $s_{\text{plane}}^{\text{rms}}$ is defined there.

20 25. Particle detectors

25.10. Superconducting solenoids for collider detectors

Revised October 1997 by R.D. Kephart (FNAL).

25.10.1. Basic (approximate) equations: In all cases SI units are assumed, so that B is in tesla, E is in joules, dimensions are in meters, and $\mu_0 = 4\pi \times 10^{-7}$.

Magnetic field: The magnetic field at the center of a solenoid of length L and radius R , having N total turns and a current I is

$$B(0,0) = \frac{\mu_0 N I}{\sqrt{L^2 + 4R^2}} . \quad (25.25)$$

Stored energy: The energy stored in the magnetic field of any magnet is calculated by integrating B^2 over all space:

$$E = \frac{1}{2\mu_0} \int B^2 dV . \quad (25.26)$$

For a solenoid with an iron flux return in which the magnetic field is $< 2T$, the field in the aperture is approximately uniform and equal to $\mu_0 N I / L$. If the thickness of the coil is small, (which is the case if it is superconducting), then

$$E \approx (\pi/2\mu_0) B^2 R^2 L . \quad (25.27)$$

Cost of a superconducting solenoid [73]:

$$\text{Cost (in M\$)} = 0.523 [(E/(1 \text{ MJ}))^{0.662}] \quad (25.28)$$

Magnetostatic computer programs: It is too difficult to solve the Biot-Savart equation for a magnetic circuit which includes iron components and so iterative computer programs are used. These include POISSON, TOSCA [74], and ANSYS [75].

25.10.2. Scaling laws for thin solenoids: For a detector in which the calorimetry is outside the aperture of the solenoid, the coil must be thin in terms of radiation and absorption lengths. This usually means that the coil is superconducting and that the vacuum vessel encasing it is of minimum real thickness and fabricated of a material with long radiation length. There are two major contributors to the thickness of a thin solenoid:

1. The conductor, consisting of the current-carrying superconducting material (usually Cu/Nb-Ti) and the quench protecting stabilizer (usually aluminum), is wound on the inside of a structural support cylinder (usually aluminum also). This package typically represents about 60% of the total thickness in radiation lengths. The thickness scales approximately as $B^2 R$.
2. Approximately another 25% of the thickness of the magnet comes from the outer cylindrical shell of the vacuum vessel. Since this shell is susceptible to buckling collapse, its thickness is determined by the diameter, length, and the modulus of the

material of which it is fabricated. When designing this shell to a typical standard, the real thickness is

$$t = P_c D^{2.5} [(L/D) - 0.45(t/D)^{0.5}] / 2.6Y^{0.4} , \quad (25.29)$$

where t = shell thickness (in), D = shell diameter (in), L = shell length (in), Y = modulus of elasticity (psi), and P_c = design collapse pressure (= 30 psi). For most large-diameter detector solenoids, the thickness to within a few percent is given by [76]

$$t = P_c D^{2.5} (L/D) / 2.6Y^{0.4} . \quad (25.30)$$

25.10.3. Properties of collider detector solenoids: The physical dimensions, central field, stored energy and thickness in radiation lengths normal to the beam line of the superconducting solenoids associated with the major colliders are given in Table 25.5.

Table 25.5: Properties of superconducting collider detector solenoids.

Experiment–Lab	Field (T)	Bore Dia (m)	Length (m)	Energy (MJ)	Thickness (X_0)
CDF–Fermilab	1.5	2.86	5.07	30	0.86
DØ –Fermilab	2.0	1.06	2.73	5.6	0.87
BaBar–SLAC	1.5	2.80	3.46	27.0	< 1.4
Topaz–KEK	1.2	2.72	5.4	19.5	0.70
Venus–KEK	0.75	3.4	5.64	12	0.52
Cleo II–Cornell	1.5	2.9	3.8	25	2.5
Aleph–CERN	1.5	5.0	7.0	130	1.7
Delphi–CERN	1.2	5.2	7.4	109	4.0
H1–DESY	1.2	5.2	5.75	120	1.2
Zeus–DESY	1.8	1.72	2.85	10.5	0.9

The ratio of stored energy to cold mass (E/M) is a useful performance measure. One would like the cold mass to be as small as possible to minimize the thickness, but temperature rise during a quench must also be minimized. Ratios as large as 8 kJ/kg may be possible (final temperature of 80 K after a fast quench with homogenous energy dump), but some contingency is desirable. This quantity is shown as a function of total stored energy for some major collider detectors in Fig. 25.6.

22 25. Particle detectors

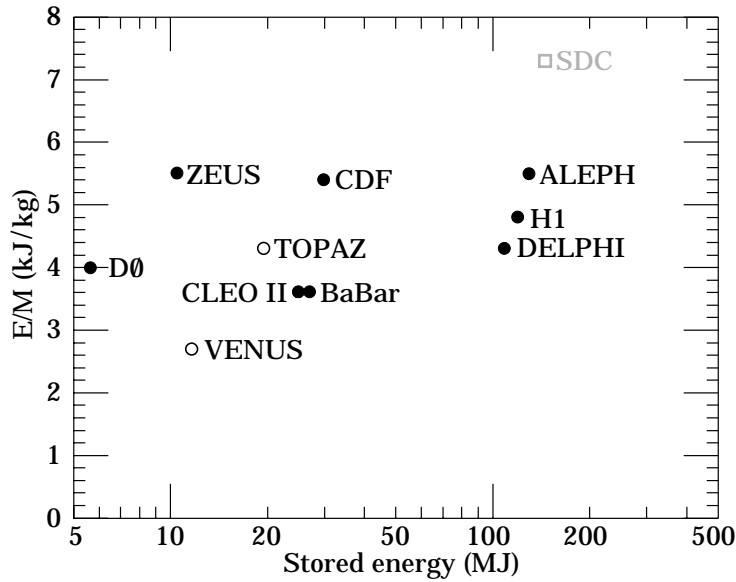


Figure 25.6: Ratio of stored energy to cold mass for existing thin detector solenoids. Solenoids in decommissioned detectors are indicated by open circles.

25.11. Other observations

dE/dx resolution in argon: Particle identification by dE/dx is dependent on the width of the distribution. For relativistic incident particles with charge e in a multiple-sample Ar gas counter with no lead [66],

$$\left. \frac{dE}{dx} \right|_{\text{FWHM}} / \left. \frac{dE}{dx} \right|_{\text{most probable}} = 0.96 N^{-0.46} (xp)^{-0.32}, \quad (25.31)$$

where N = number of samples, x = thickness per sample (cm), p = pressure (atm.). Most commonly used chamber gases (except Xe) give approximately the same resolution.

Free electron drift velocities in liquid ionization chambers [67–70]: Velocity as a function of electric field strength is given in

References:

1. *Experimental Techniques in High Energy Physics*, T. Ferbel (ed.) (Addison-Wesley, Menlo Park, CA, 1987).
2. J.B. Birks, *The Theory and Practice of Scintillation Counting* (Pergamon, London, 1964).
3. D. Clark, *Nucl. Instrum. Methods* **117**, 295 (1974).
4. B. Bengston and M. Moszynski, *Nucl. Instrum. Methods* **117**, 227 (1974); J. Bialkowski *et al.*, *Nucl. Instrum. Methods* **117**, 221 (1974).

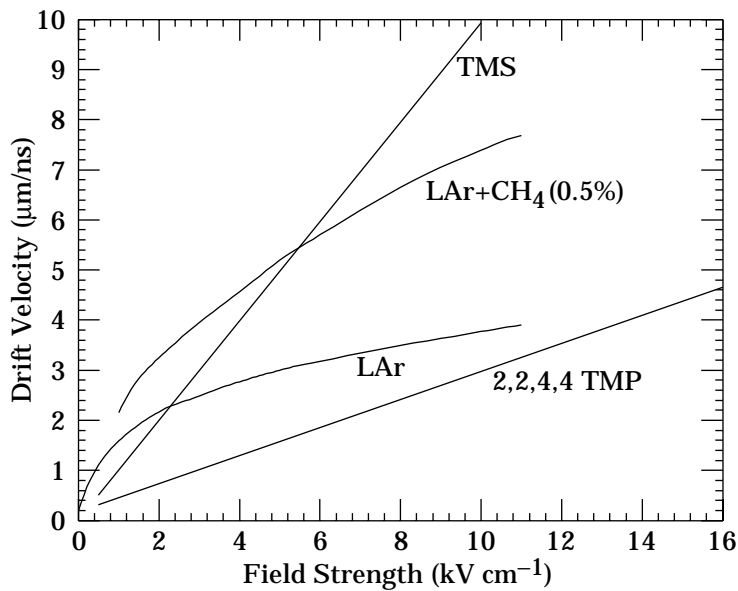


Figure 25.7: Electron drift velocity as a function of field strength for commonly used liquids.

5. *Proceedings of the Symposium on Detector Research and Development for the Superconducting Supercollider*, eds. T. Dombeck, V. Kelly and G.P. Yost (World Scientific, Singapore, 1991).
6. I.B. Berlman, *Handbook of Fluorescence Spectra of Aromatic Molecules*, 2nd edition (Academic Press, New York, 1971).
7. C. Zorn in *Instrumentation in High Energy Physics*, ed. F. Sauli, (1992, World Scientific, Singapore) pp. 218–279.
8. T. Foerster, *Ann. Phys.* **2**, 55 (1948).
9. J.B. Birks, *Proc. Phys. Soc.* **A64**, 874 (1951).
10. J.B. Birks, *The Theory and Practice of Scintillation Counting*, Chapter 6, (Pergamon, London, 1964);
J.M. Fluornoy, *Conference on Radiation-Tolerant Plastic Scintillators and Detectors*, K.F. Johnson and R.L. Clough editors, *Rad. Phys. and Chem.*, **41** 389 (1993).
11. D. Horstman and U. Holm, *ibid* 395.
12. D. Blomker *et al.*, *Nucl. Instrum. Methods* **A311**, 505 (1992);
J. Mainusch *et al.*, *Nucl. Instrum. Methods* **A312**, 451 (1992).
13. *Conference on Radiation-Tolerant Plastic Scintillators and Detectors*, K.F. Johnson and R.L. Clough editors, *Rad. Phys. and Chem.*, **41** (1993).
14. R.K. Swank, *Ann. Rev. Nucl. Sci.* **4**, 137 (1954);
G.T. Wright, *Proc. Phys. Soc.* **B68**, 929 (1955).

24 25. Particle detectors

15. M. Laval *et al.*, Nucl. Instrum. Methods **206**, 169 (1983).
16. M. Moszynski *et al.*, Nucl. Instrum. Methods **A226**, 534 (1984).
17. E. Blucher *et al.*, Nucl. Instrum. Methods **A249**, 201 (1986).
18. C. Bebek, Nucl. Instrum. Methods **A265**, 258 (1988).
19. S. Kubota *et al.*, Nucl. Instrum. Methods **A268**, 275 (1988).
20. B. Adeva *et al.*, Nucl. Instrum. Methods **A289**, 35 (1990).
21. I. Holl, E. Lorentz, G Mageras, IEEE Trans. Nucl. Sci. **35**, 105 (1988).
22. J. Litt and R. Meunier, Ann. Rev. Nucl. Sci. **23**, 1 (1973).
23. D. Bartlett *et al.*, Nucl. Instrum. Methods **A260**, 55 (1987).
24. P. Duteil *et al.*, Review of Scientific Instruments **35**, 1523 (1964).
25. M. Cavalli-Sforza *et al.*, Construction and Testing of the SLC Čerenkov Ring Imaging Detector, IEEE **37**, N3:1132 (1990).
26. E.G. Anassontzis *et al.*, Recent Results from the DELPHI Barrel Ring Imaging Cherenkov Counter, IEEE **38**, N2:417 (1991).
27. R.T. Rewick *et al.*, Anal Chem **60**, 2095 (1989).
28. B. Dolgoshein, "Transition Radiation Detectors," Nucl. Instrum. Methods **A326**, 434 (1993).
29. X. Artru *et al.*, Phys. Rev. **D12**, 1289 (1975).
30. G.M. Garibian *et al.*, Nucl. Instrum. Methods **125**, 133 (1975).
31. RD6 Collaboration, CERN/DRDC 90-38 (1990); CERN/DRDC 91-47 (1991); CERN/DRDC 93-46 (1993).
32. ATLAS Collaboration, ATLAS Inner Detector Technical Design Report, Volume 2, ATLAS TDR 5, CERN/LHCC/97-16 (30 April 1997).
33. B. Dolgoshein, Nucl. Instrum. Methods **252**, 137 (1986).
34. C.W. Fabjan *et al.*, Nucl. Instrum. Methods **185**, 119 (1981).
35. J. Cobb *et al.*, Nucl. Instrum. Methods **140**, 413 (1977).
36. A. Büngener *et al.*, Nucl. Instrum. Methods **214**, 261 (1983).
37. R.D. Appuhn *et al.*, Nucl. Instrum. Methods **263**, 309 (1988).
38. Y. Watase *et al.*, Nucl. Instrum. Methods **248**, 379 (1986).
39. R. Ansari *et al.*, Nucl. Instrum. Methods **263**, 51 (1988).
40. H.J. Butt *et al.*, Nucl. Instrum. Methods **252**, 483 (1986).
41. J.F. Detoeuf *et al.*, Nucl. Instrum. Methods **265**, 157 (1988).
42. M. Holder *et al.*, Nucl. Instrum. Methods **263**, 319 (1988).
43. H. Weidkamp, DiplomArbeit, Rhein-Westf. Tech. Hochschule Aachen (1984).
44. H. Grässler *et al.*, Proc. Vienna Wire Chamber Conference (1989).
45. T. Akesson *et al.*, CERN Preprint, CERN-PPE/97-161 (1997), to be published in Nucl. Instr. and Meth.
46. T. Trippe, CERN NP Internal Report 69-18 (1969).
47. S. Parker and R. Jones, LBL-797 (1972);

- P. Morse and H. Feshbach, *Methods of Theoretical Physics*, McGraw-Hill, New York, 1953, p. 1236.
48. D.R. Nygren and J.N. Marx, "The Time Projection Chamber", *Phys. Today* **31**, 46 (1978).
 49. W. Blum and L. Rolandi, *Particle Detection with Drift Chambers*, Springer-Verlag (1994).
 50. W.R. Nelson, H. Hirayama and D.W.O. Rogers, "The EGS4 Code System," SLAC-265, Stanford Linear Accelerator Center (Dec. 1985).
 51. D. Hitlin *et al.*, *Nucl. Instrum. Methods* **137**, 225 (1976). See also W. J. Willis and V. Radeka, *Nucl. Instrum. Methods* **120**, 221 (1974), for a more detailed discussion.
 52. E. Bloom and C. Peck, *Ann. Rev. Nucl. and Part. Sci.* **33**, 143 (1983).
 53. M.A. Akrawy *et al.*, *Nucl. Instrum. Methods* **A290**, 76 (1990).
 54. H. Burkhardt *et al.*, *Nucl. Instrum. Methods* **A268**, 116 (1988).
 55. W. Hoffman *et al.*, *Nucl. Instrum. Methods* **163**, 77 (1979).
 56. M.A. Schneegans *et al.*, *Nucl. Instrum. Methods* **193**, 445 (1982).
 57. C. Fabjan and R. Wigmans, *Rept. Prog. Phys.* **52**, 1519 (1989).
 58. J.V. Allaby *et al.*, *Nucl. Instrum. Methods* **A281**, 291 (1989).
 59. R. Wigmans, *Nucl. Instrum. Methods* **A259**, 389 (1987).
 60. R. Wigmans, *Nucl. Instrum. Methods* **A265**, 273 (1988).
 61. D. Bintinger, in *Proceedings of the Workshop on Calorimetry for the Supercollider*, Tuscaloosa, AL, March 13–17, 1989, edited by R. Donaldson and M.G.D. Gilchriese (World Scientific, Teaneck, NJ, 1989), p. 91.
 62. T.A. Gabriel, D.E. Groom, P.K. Job, N.V. Mokhov, and G.R. Stevenson, *Nucl. Instrum. Methods* **A338**, 336 (1994).
 63. R.K. Bock, T. Hansl-Kozanecka, and T.P. Shah, *Nucl. Instrum. Methods* **186**, 533 (1981).
 64. T. Akesson *et al.*, *Nucl. Instrum. Methods* **A262**, 243 (1987).
 65. E. Bernardi *et al.*, *Nucl. Instrum. Methods* **A262**, 229 (1987).
 66. W.W.M. Allison and J.H. Cobb, "Relativistic Charged Particle Identification by Energy-Loss," *Ann. Rev. Nucl. Sci.* **30**, 253 (1980), see p. 287.
 67. E. Shibamura *et al.*, *Nucl. Instrum. Methods* **131**, 249 (1975).
 68. T.G. Ryan and G.R. Freeman, *J. Chem. Phys.* **68**, 5144 (1978).
 69. W.F. Schmidt, "Electron Migration in Liquids and Gases," HMI B156 (1974).
 70. A.O. Allen, "Drift Mobilities and Conduction Band Energies of Excess Electrons in Dielectric Liquids," NSRDS-NBS-58 (1976).
 71. R.L. Gluckstern, *Nucl. Instrum. Methods* **24**, 381 (1963).
 72. V. Karimäki, *Nucl. Instrum. Methods* **A410**, 284 (1998).
 73. M.A. Green, R.A. Byrns, and S.J. St. Lorant, "Estimating the cost of superconducting magnets and the refrigerators needed to keep them cold," in *Advances in Cryogenic Engineering*, Vol. 37, Plenum Press, New York (1992).

26 *25. Particle detectors*

74. Vector Fields, Inc., 1700 N. Farnsworth Ave., Aurora, IL.
75. Swanson Analysis Systems, Inc., P.O. Box 65, Johnson Rd., Houston, PA.
76. CGA-341-1987, "Standard for insulated cargo tank specification for cryogenic liquids," Compressed Gas Association, Inc., Arlington, VA (1987).